Benchmark study on motions and loads of a 6750-TEU containership

Yonghwan Kim *, Jung-Hyun Kim

Department of Naval Architecture & Ocean Engineering, Seoul National Univ., 1, Gwanak-ro, Gwanak-gu, Seoul 151-744, Republic of Korea

A B S T R A C T

This study deals with a benchmark test on the performance of seakeeping analysis codes, which was carried out as part of the 2nd ITTC–ISSC joint workshop in 2014. Eleven institutes participated in the benchmark test with seventeen analysis codes. The target ship was the 6750-TEU containership, and the test of its flexible scale model was conducted by KRISO. A test matrix was composed of one condition for linear responses and three conditions for nonlinear responses. Participants were requested to conduct computational simulations and submit their heave, pitch, and vertical bending moment results in head regular waves. The computational results obtained are compared with each other using statistical analysis. The comparison reveals the performances and trends of the computational results. In addition, all the model data is included in the paper in order to encourage readers to participate in the benchmark test.

© 2016 The Authors. Published by Elsevier Ltd. This is an open access article under the CC BY-NC-ND license (http://creativecommons.org/licenses/by-nc-nd/4.0/).

1. Introduction

Seakeeping analysis is an essential measure for researchers in the field of ship hydrodynamics because motion performance is critical for operational and structural safety. The experimental method is considered reliable, but it is time-consuming and expensive. Analytical or numerical analysis methods have thus been developed as an alternative. The first meaningful attempt at seakeeping analysis was initiated by Kriloff (1896) based on Froude–Kriloff hypothesis, which assumes that a hydrodynamic force is only induced by an undisturbed incident wave. Fifty years later, diffraction and radiation problems were solved by Havelock (1942), Haskind (1946) and Ursell (1949) using a velocity potential. Those works were based on a 2D method with a linear assumption. They were improved using various forms of slender-body and strip theories and widely used in seakeeping analysis (Korvin-Kroukovsky and Jacobs, 1957; Newman, 1964; Ogilvie and Tuck, 1969; Salvesen et al., 1970). In order to compensate for the insufficient solutions of strip theory in long wave lengths and slender-body theory in short wave lengths, a unified theory was developed (Maruo, 1970; Newman and Sclavounos, 1980; Kashiwagi, 1995). The above methods yield quite good results for a seakeeping analysis, but they cannot completely overcome limitations due to the application of a 2D method to a 3D problem. In order to cope with the limitations, a 3D boundary element method

(BEM) was initially attempted by Hess and Smith (1962). 3D BEM uses either a wave Green's function or a Rankine source as a source potential to satisfy boundary conditions. The most well-known program for seakeeping analysis is WAMIT, which uses a wave Green's function in the frequency domain (Korsmeyer et al., 1988). Many of the frequency domain methods were extended to include a time domain analysis using the method of Cummins (1962), the so-called impulse response function (IRF) approach. 3D BEM using a Rankine source is preferred in a time domain such as SWAN (Nakos and Sclavounos, 1990; Kring, 1994), LAMP (Lin and Yue, 1991), and WISH (Kim et al., 2011), which have advantages in consideration of forward speed and nonlinearity. Recently, computational fluid dynamics (CFD) methods were also applied to seakeeping analyses; these methods have great advantages in the simulation of viscous or violent flow (Gentaz et al., 1999; Sadat-Hosseini et al., 2013; Yang et al., 2013).

The hydroelastic approach is one of the important branches of the seakeeping analysis method. The hydroelastic approach should be used when the ship is exposed to wave-induced vibration, referred to as springing and whipping. Wave-induced vibration plays a role in structural response, if it occurs. The hydroelastic approach to seakeeping analysis was first attempted by Belgova (1962). It was established in the work of Bishop and Price (1979). The key point of the hydroelastic approach is that distortions associated with structural modes, such as vertical/horizontal bending and torsion, are obtained in addition to the six motions of a rigid body. Recently, various hydroelastic methods of seakeeping analysis were tried with partial or full consideration of nonlinearity (Jensen and Dogliani, 1996; Malenica and Tuitman, 2008; Iijima et al., 2008; Kim et al., 2009; Oberhagemann and Moctar, 2012). The

* Corresponding author.
E-mail addresses: yhwankim@snu.ac.kr (Y. Kim),
wowplusme@snu.ac.kr (J.-H. Kim).

most practical method to date might be a combination of 3D BEM, 3D finite element method (FEM), and a 2D slamming model, which are coupled with each other via eigenvectors of 3D FEM (Kim et al., 2015).

According to the above histories of seakeeping analysis methods, the development of seakeeping analysis methods is on a trend toward a combination of 3D modeling, time domain, and nonlinear methods. A comparative or benchmark study on the current methods of seakeeping analysis is needed to investigate the current status and define a development direction for the future. To meet the demand, an International Towing Tank Conference (ITTC) committee conducted a comparative study on ship motions and loads for the S175 containership in 1978 (ITTC, 1978). The ITTC study focused on motion predictions for forward speed by strip theories. Cooperative Research Ships (CRS) also conducted a comparative study on a containership (Bunnik et al., 2010). The CRS study included results of various methods and categorized them into five groups: approximate forward speed (AFS), exact forward speed (EFS), double body (DB), nonlinear steady (NLS), and computational fluid dynamics (CFD) methods. Another comparative study on the S175 containership was performed by one of the authors as part of ITTC workshop on seakeeping in 2010. The study compared both linear and nonlinear motions and loads.

This paper presents a benchmark study on ship motions and loads for a 6750-TEU containership, which was carried out by ITTC and International Ship and Offshore Structures Congress (ISSC) members. The result was presented at the 2nd ITTC–ISSC joint workshop in Copenhagen, Denmark, 30 August 2014. An experimental result including hydroelasticity was provided by Korea Research Institute of Ships and Ocean Engineering/Korea Institute of Ocean Science and Technology (KRISO/KIOST). A test matrix was constructed for an investigation on performances of seakeeping analysis methods, which are related to wave frequency, forward speed, nonlinear vertical bending moment, and hydroelasticity. An attempt was made to compare the computational results from a statistical point of view. The average of the computational results was used as the reference value and compared with the experimental result. The standard deviation of the computational results implies a difficulty in the computational methods. The difficulty are related with numerical errors, incompleteness of background theory, or user's mistake. For example, if a problem to be solved is nonlinear and sensitive to discretization, solutions obtained by various grids and methods will be scattered more than those of a linear and non-sensitive problem.

2. Outline of benchmark test

The benchmark test was carried out to assess performances and trends of seakeeping analysis codes as part of the ITTC–ISSC joint workshop in 2014. Eleven institutes participated in the benchmark test with seventeen analysis codes. The ship data of the 6750-TEU containership and the test matrix were offered to the participants. The participants were requested to compute simulations and submit their best results for comparison. The test matrix was composed of one condition for linear response amplitude operators (RAO) and three conditions for nonlinear responses. The ship was exposed to head regular waves for all the conditions. This paper provides all the information of the benchmark test and helps readers join the benchmark test.

2.1. Target ship

The 6750-TEU containership was chosen as the target ship of the benchmark test, and its experimental result was provided by KRISO. The experimental model of the containership was
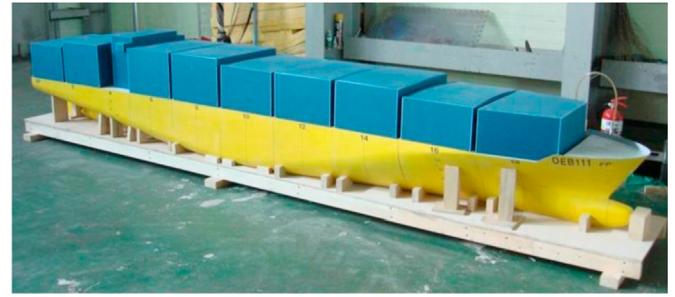

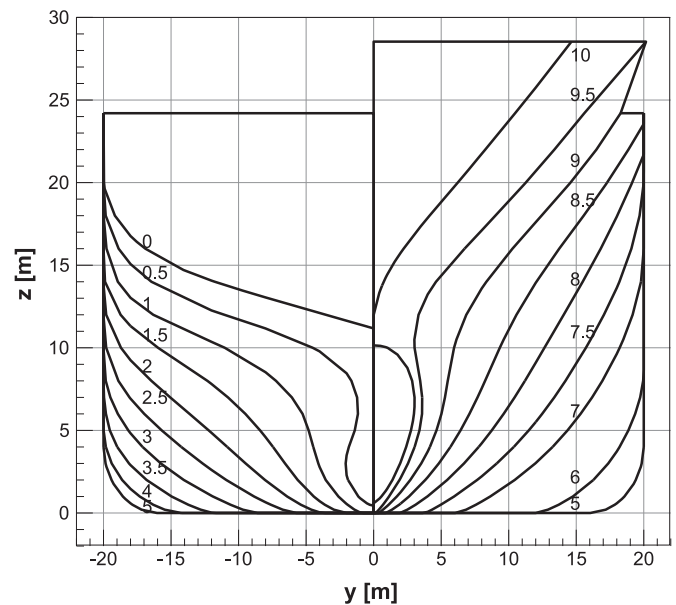**Fig. 1.** Experimental model of the 6750-TEU containership.

Fig. 2. Body plan of the 6750-TEU containership.

Table 1
Principal dimensions of the 6750-TEU containership.

Item	Real scale	Model scale
Scale	1/1	1/70
LOA (m)	300.891	4.298
LBP (m)	286.6	4.094
Breadth (m)	40	0.571
Height (m)	24.2	0.346
Draft at AP and FP (m)	11.98	0.171
Displacement	85,562.7 t	249.454 kg
KM (m)	18.662	0.267
GM (m)	2.1	0.03
KG (m)	16.562	0.237
LCG from AP (m)	138.395	1.977
kxx (m)	14.6	0.206
kyy (m)	70.144	1.002
kzz (m)	70.144	1.002
Natural Period of Roll (s)	20.5	2.45
Neutral axis from keel (m)	7.35	0.105

constructed using a flexible backbone and segmented hulls as shown in Fig. 1. The body plan of the containership is illustrated in Fig. 2. The station number is 0 at AP and 10 at FP. Principal dimensions of the containership are given in Table 1. The containership consists of eight segmented hulls and inertial properties of the segmented hulls are presented in Table 2. The reference of LCG is the left end of each segment, and the reference of gyration radius kxx (roll), kyy (pitch), and kzz (yaw) is LCG and KG of each segment. Each segment is connected to the backbone via a fixing system as shown in Fig. 3. Six motions are measured at the mass

Table 2
Inertial properties of each segmented hull (real scale).

Segment ID	Mass (ton)	LCG (m)	KG (m)	kxx (m)	kyy (m)	kzz (m)
1	10,326.087	31.989	16.562	14.6	13.053	13.053
2	4844.12	11.275	16.562	14.6	7.61	7.61
3	10,042.864	16.318	16.562	14.6	9.092	9.092
4	11,902.906	14.551	16.562	14.6	10.429	10.429
5	12,322.063	17.094	16.562	14.6	11.835	11.835
6	10,869.002	15.18	16.562	14.6	12.919	12.919
7	9406.402	15.72	16.562	14.6	14.008	14.008
8	15,849.258	29.303	16.562	13.486	23.698	23.698
Total	85,562.7	138.395	16.562	14.4	70.144	70.144

center using RODYM6D and NI 6031E. Sectional forces are measured at seven sections by strain gauges installed on the backbone and NI 9237. Each section has two strain gauges at neutral axis and one at the center line of the backbone. Principal dimensions of the backbone are given in Table 3. The fixing system consists of upper and lower supporting plates that press the surfaces of the backbone as shown in Fig. 4. The supporting plates have a rectangular shape except the lower plate of Segment 1 and the upper and lower plates of Segment 8. Breadth, longitudinal extent, and thickness of the upper and lower plates are 140 mm × 100 mm × 10 mm and 180 mm × 100 mm × 10 mm, respectively. The shapes of the lower plate of Segment 1 and the lower and upper plates of Segment 8 are isosceles trapezoids of 100 mm × 150 mm × 220 mm × 10 mm (shorter breadth × longer breadth × longitudinal extent × thickness). The fixing system is expected to slightly increase the bending rigidity of the backbone by constraint of deflection. The natural frequency of two-node vertical bending is given in Table 4. A numerical model can be constructed using the given data, and it should be confirmed that the natural frequency of two-node vertical bending is the same in both the experimental and numerical models.

2.2. Test conditions

The condition for linear response amplitude operator (RAO) is named RAO, and the three conditions for nonlinear responses are named NL1, NL2, and NL3. The details of the conditions are given Table 5. These conditions are selected from the test matrix of the experiment. Thus, the experimental results of the conditions are available to be compared with computational results. The test condition of RAO is planned for the investigation on the relationship between wave frequencies and differences of computational results without forward speed. In the RAO condition, the participants are required to provide RAOs of heave, pitch, and vertical bending moment (VBM) at Section 4. The test condition of NL1 is prepared for a comparison of nonlinear VBM distribution for a relatively mild wave condition. The test condition of NL2 corresponds to a severe case of the ship exposed to nonlinear springing and slamming-whipping. Hydroelasticity of the ship

Table 3
Principal dimensions of backbone.

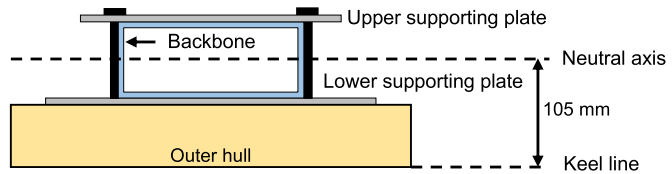| Backbone	Real scale (m)	Model scale (mm)
B	7.000	100.000
H	3.500	50.000
t	0.161	2.300
Young's modulus, E	14 (TPa)	200 (GPa)
Bending stiffness, EI	100.08 (m^4 TPa)	59,546.438 (mm^4 TPa)
Neutral axis from keel	7.350	105.000

Fig. 4. Fixing system of the backbone.

Table 4
Natural frequencies of the experimental model.

Mode	Natural frequency of two-node vertical bending	
	Real scale (Hz)	Model scale (Hz)
Dry mode	0.785	6.571
Wet mode	0.645	5.4

should be considered in computation of NL2. The test condition of NL3 is selected to examine the effect of forward speed. The participants are requested to submit time series of heave, pitch, and VBM at Section 4 ($x/L=0.43$) and the maximum hogging and sagging moments at Sections 1-7 in the nonlinear conditions. The still water load is not included in results.

2.3. Participants

A total of seventeen codes participated in the benchmark test from eleven institutes. The details of the participants are given in Table 6. Sixty percent of the participants are based on a 3D BEM. 3D BEM is currently considered the most common method for seakeeping analysis. The participants are categorized in terms of nonlinear extension, computational domain, and commercialization as shown in Table 7. Seventy six percent of the participants support nonlinear computation and have commercial licenses. A total of 70% of the participants conduct simulations in a time domain. The heave and pitch results of Participants 1, 2, 3, 7, 9, 15, and 16 were not submitted for the cases of NL1, NL2, and NL3. Longitudinal VBM distributions of Participants 1, 7, 9, 15, and 16 were not submitted for the cases of NL1, NL2, and NL3. In addition, a longitudinal VBM distribution of Participant 10 is excluded from a comparison because the data seems to be incorrect.
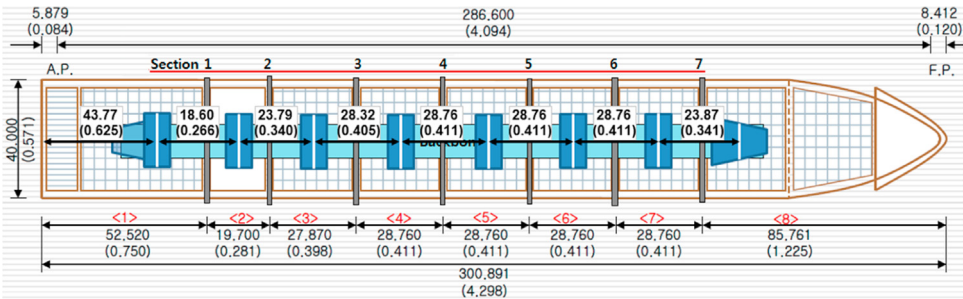

Fig. 3. Configuration of the backbone and segmented hulls.

Table 5
Test conditions for benchmark test (real scale).

Test ID	Wave freq.(rad/s)	λ/L	Wave height (m)	H/λ	Heading angle (deg)	Forward speed (m/s)	Froude no.
RAO	0.242–0.628	0.54–3.68	Small value	< 1/100	180	0	0
NL1	0.449	1.07	6.118	1/50	180	2.572	0.05
NL2	0.449	1.07	10.926	1/28	180	2.572	0.05
NL3	0.449	1.07	6.118	1/50	180	6.173	0.12

Table 6
List of participants.

ID	Institutes	Codes	Method	LIN	NL
1	CSSRC (China Ship Scientific Research Center)	THAFTS	3D BEM (WGF)	O	X
2	DNV GL (Det Norske Veritas Germanischer Llyod)	GL Rankine1	3D BEM (Rankine)	O	O
3		GL Rankine2	3D BEM (WGF)	O	O
4	HEU (Harbin Engineering University)	COMPASS-WALCS-LE/NE	3D BEM (WGF)	O	O
5	IST (Instituto Superior Tecnico)	In-house	Strip	O	O
6	LR (Llyod's Register)	CRS PRECAL, PRETTI, TDWHIP	3D BEM (WGF)	O	O
7	MUN (Memorial University of Newfoundland)	MAPS0	Panel-Free Method (potential flow)	O	X
8	NMRI (National Maritime Research Institute)	NMRIW	Strip	O	O
9	NTUA (National Technical University of Athens)	NEWDRIFT	3D BEM (WGF)	O	X
10		HYBRID	IRF	X	O
11	SNU (Seoul National University)	WISH	3D BEM (Rankine)	O	O
12		WISH-FLEX 3DM	3D BEM (Rankine)	O	O
13		WISH-FLEX BEAM	3D BEM (Rankine)	O	O
14	UDE (University of Duisberg-Essen)	COMET	RANSE	O	O
15	UZUR (University of Zagreb and University of Rijeka)	Waveship	Strip	O	X
16		HydroSTAR	3D BEM (WGF)	O	O
17		Gretel	Strip	O	O

Table 7
Categorization of participants.

Category	Nonlinear Extension		Computational Domain		Commercialization	
	Linear	Nonlinear	Frequency	Time	Commercial	In-house
No. of Codes	4	13	5	12	13	4

2.4. Hydrostatic component

The participants are required to submit hydrostatic components of their numerical models. The submerged volume in still water is compared in Fig. 5. The reference value is calculated by dividing the total mass by fluid density, which is plotted by the horizontal line at 85,563 m³ of the vertical axis. All the results show acceptable differences, and the maximum difference is −3.3%. Centers of buoyancy of the participants are located between −1.5% (toward AP) and +3.4% (toward FP) of LBP from LCG as shown in Fig. 6. Some computational results might induce trim though there is no trim in the given model data.

3. Comparison of result

Statistical values are obtained for a comparison of the experimental and computational results. The used statistical values are explained below.
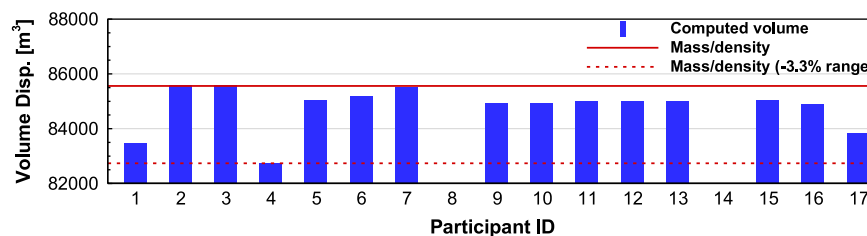
- Mean: the average of computational results.
- Min. and Max.: the minimum and maximum values of computational results.
- SD: the standard deviation of computational results.
- Mean $\pm$ SD: the standard deviation range of computational results.

Mean and Mean $\pm$ SD are calculated as

$$\text{Mean} = \frac{\sum_{i=1}^{N} R_i}{N} \tag{1}$$

$$\text{Mean} \pm \text{SD} = \text{Mean} \pm \sqrt{\frac{\sum_{i=1}^{N} (\text{Mean} - R_i)^2}{N}} \tag{2}$$

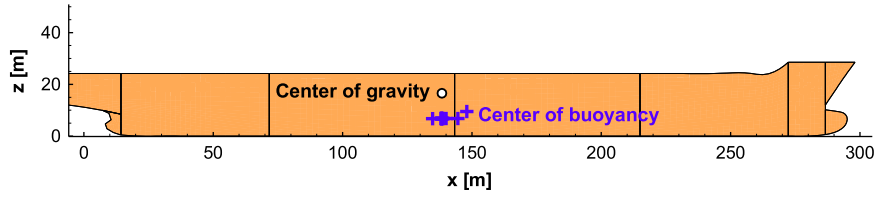**Fig. 5.** Comparison of submerged volume in still water.

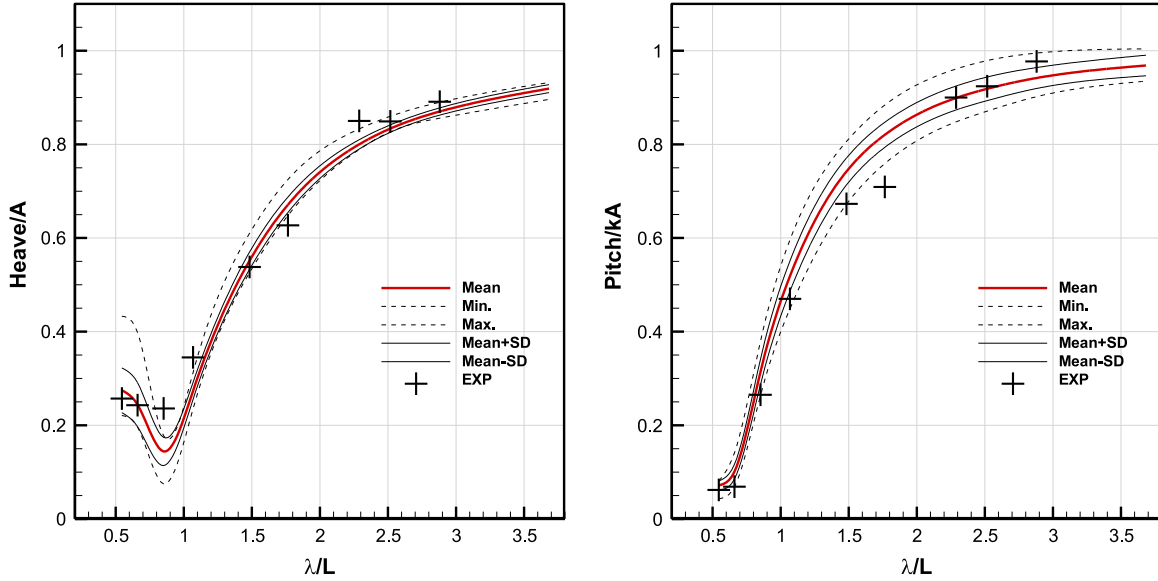**Fig. 6.** Comparison of center of buoyancy in still water.

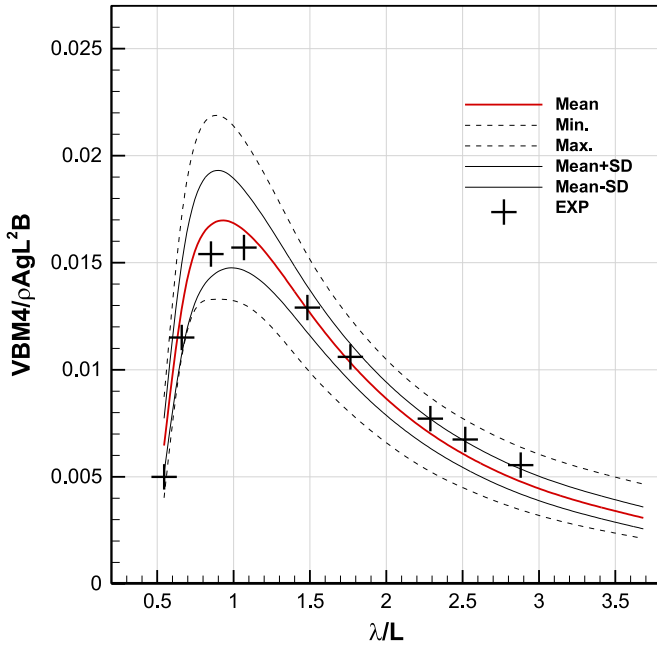**Fig. 7.** Comparison of heave and pitch RAOs.

Fig. 8. Comparison of VBM RAO at Section 4.

where R_i is the computational result of the i-th participant and N is the total number of participants. The statistical values are also compared with each other and the experimental result. In comparison of time series, Min., Max., and Mean are extracted at each time step, and the extracted values are plotted along the time axis as the time series.

In addition, total and amplitude differences of the i-th participant are defined as

$$\text{Total Difference}_i\ [\%] = \frac{\sum_{j=1} \left| R_i{}^j - \text{Mean}^j \right|}{\sum_{j=1} \text{Mean}^j} *100$$

$$(j = 1 - 10:\ 0.54 - 3.68\lambda/L \text{ or } 1 - 7:\ 0.16 - 0.73\ x/L) \qquad (3)$$

$$\text{Amplitude Difference}_i\left[\%\right] = \frac{|R_i - \text{Mean}|}{\text{Mean}} *100 \qquad (4)$$

where $R_i{}^j$ is the computational result of the j-th component of the i-th participant and Mean^j is the average of the j-th component. The total difference is used to compare linear RAOs and nonlinear sagging and hogging moments, which have multiple values in the results. The amplitude difference is used to compare single values of amplitudes of nonlinear heave and pitch motions.

3.1. Linear response

The first step is to compare linear responses to head seas. Heave and pitch RAOs are compared in Fig. 7. A quite good agreement is observed when $\lambda/L > 1.0$ in the computational result of heave according to the small value of standard deviation. On the other hand, the standard deviations of the pitch motion are not small when $\lambda/L > 1.0$ as compared to that of heave. The VBM RAO is compared in Fig. 8 The VBM shows a large standard deviation compared to those of the heave and pitch motions. The peak is observed at $\lambda/L = 1.0$. Overall, the experimental results are close to the average of the computational results.

The total differences of the heave, pitch, and VBM RAOs are compared in Figs. 9–11. The total differences of heave are smaller than 4% with the exception of Participant 17. In the result of pitch, the
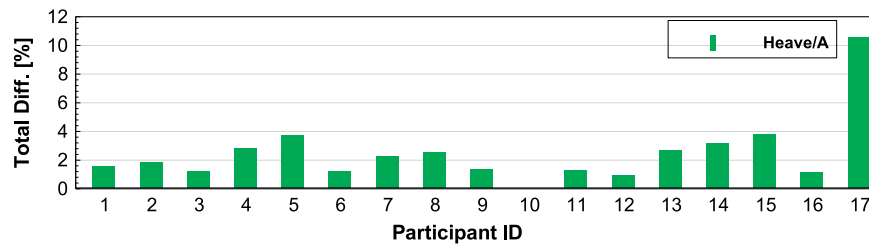
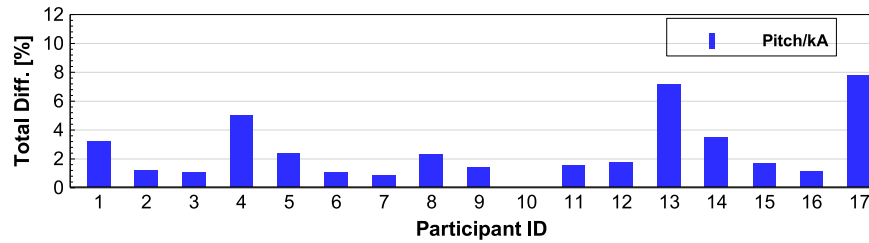**Fig. 9.** Total differences of heave RAO.

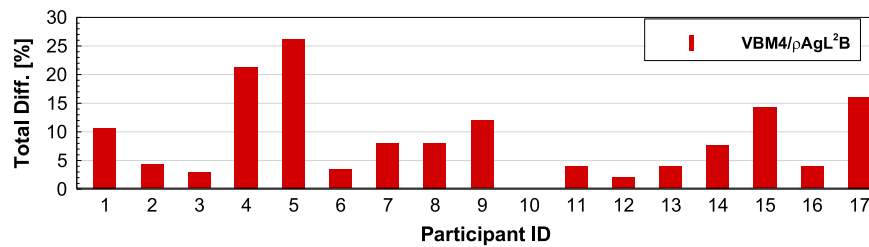**Fig. 10.** Total differences of pitch RAO.

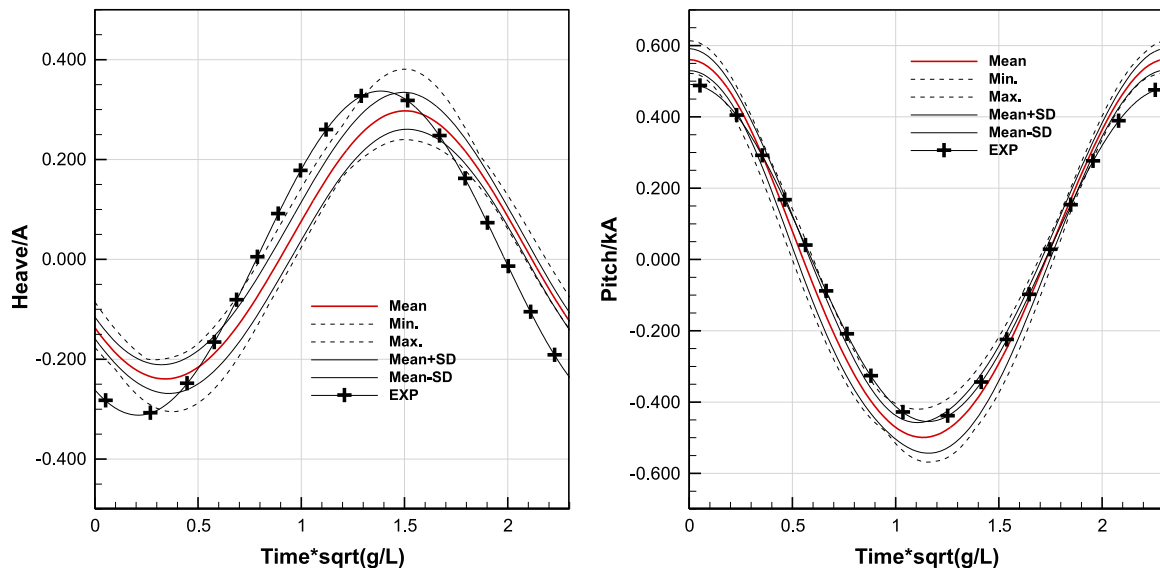**Fig. 11.** Total differences of VBM RAO.

Fig. 12. Comparison of heave and pitch in NL1.

total differences are within 8%. It can be considered that all the computational results show good agreement in heave and pitch RAOs. However, the total differences of VBM are larger than those of heave and pitch motions. Six participants show differences larger than 10% and two participants show differences larger than 20%. It can be seen that the difference of heave is more related with the difference of VBM than that of pitch by observing the differences of

Participants 4, 5, 15, and 17. Participants 3, 6, 11, 12, and 16 show smaller differences in all the RAOs, and Participants 4, 5, 13, and 17 show larger differences in either heave, pitch, or VBM RAO.

3.2. Nonlinear response: NL1

The test case of NL1 is not a highly nonlinear condition. It is prepared for a comparison of a nonlinear VBM distribution in a
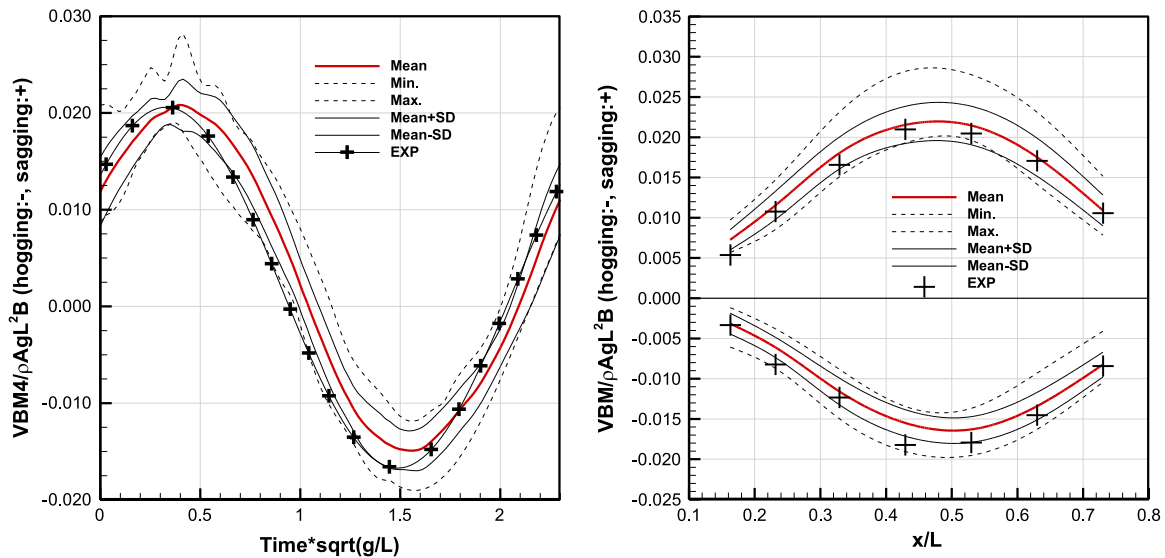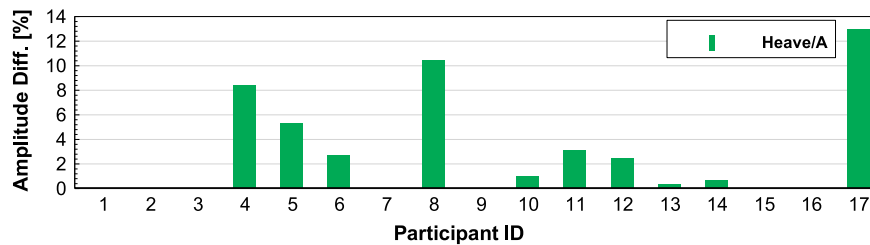
Fig. 13. Comparison of VBM in NL1.

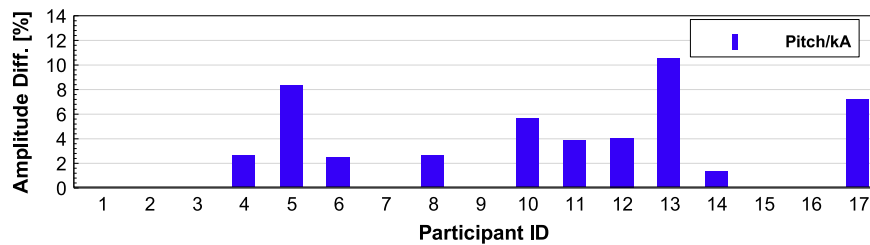**Fig. 14.** Amplitude differences of heave in NL1.

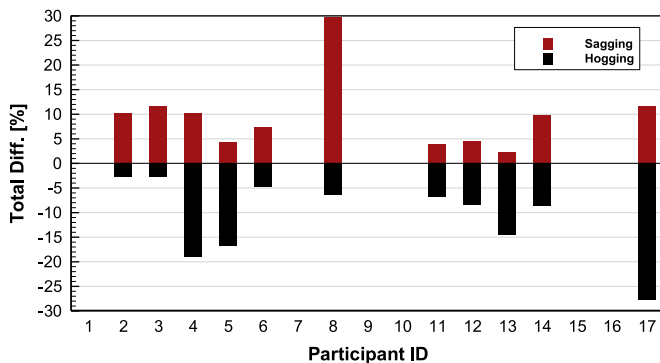**Fig. 15.** Amplitude differences of pitch in NL1.

Fig. 16. Total differences of hogging and sagging moments in NL1.

relatively mild wave condition. The time series of heave, pitch, and VBM at Section 4 are compared in Figs. 12 and 13. It should be noted that the time series are shifted to match the positive peaks of pitch motions at 0.0 s. A time lag is very small between the computational results, whereas it is non-negligible between the experimental and computational results. The time lag might be

due to a difference of inertial property between the numerical and experimental models because there is no difference in the inertial properties of the numerical models. Unfortunately, the experimental data was not enough to assess an error in inertial property. The numerical results tend to underestimate heave and VBM and overestimate pitch compared to the experimental result. Longitudinal distributions of sagging and hogging moments are compared in Fig. 13 (right). The maximum calculated sagging moment is about 30% larger than the maximum calculated hogging moment. The difference between sagging and hogging moments is considered by the integration of pressure on the instantaneously wetted surface in the computation. It can be partly considered by a weakly nonlinear approach or fully considered by fully nonlinear method such as CFD. The experiment estimates similar sagging moments and larger hogging moments compared to the average of the computational results.

The amplitudes of the differences of heave and pitch are compared in Figs. 14 and 15. The maximum differences of heave and pitch are about 13% and 10%, respectively. The total differences of sagging and hogging are compared in Fig. 16. The maximum differences of sagging and hogging moments are about 30% and 27%, respectively.
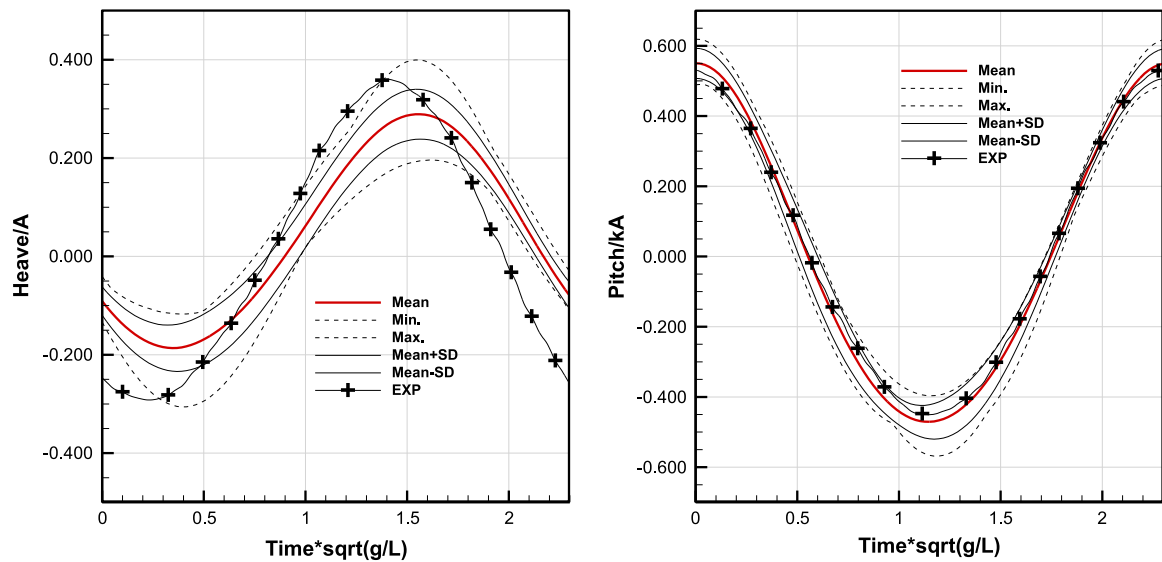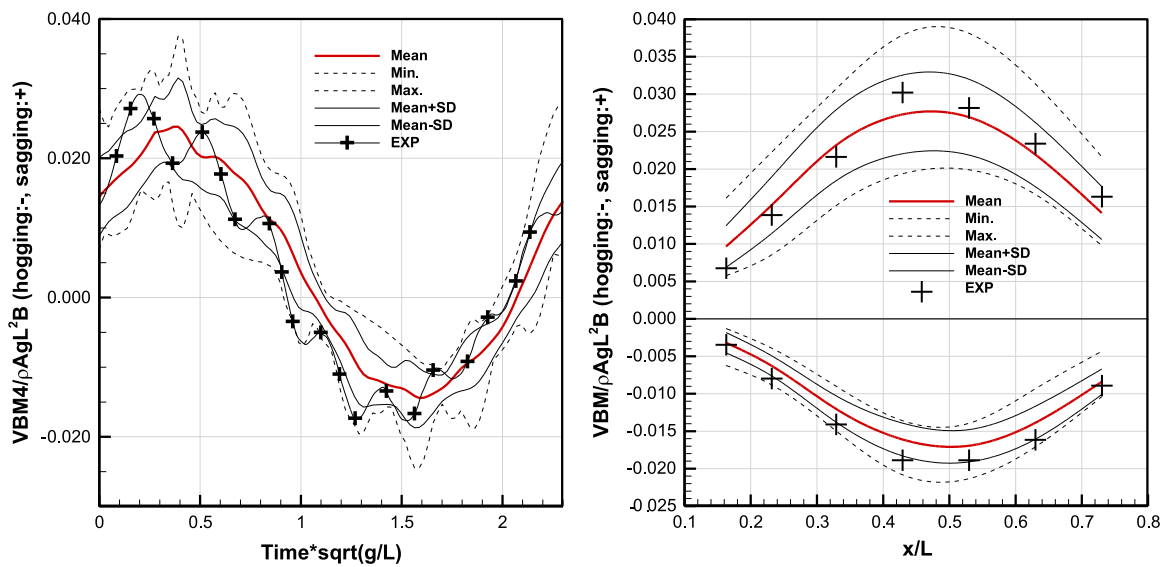
Fig. 17. Comparison of heave and pitch in NL2.

Fig. 18. Comparison of VBM in NL2.
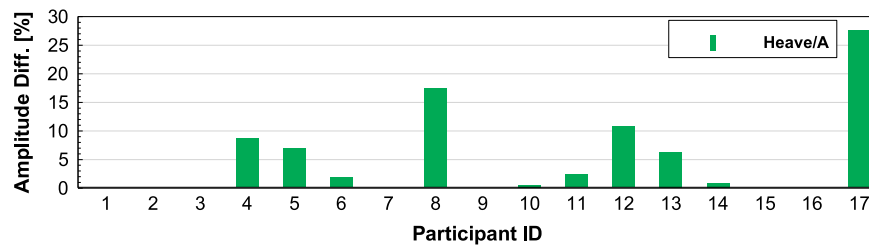

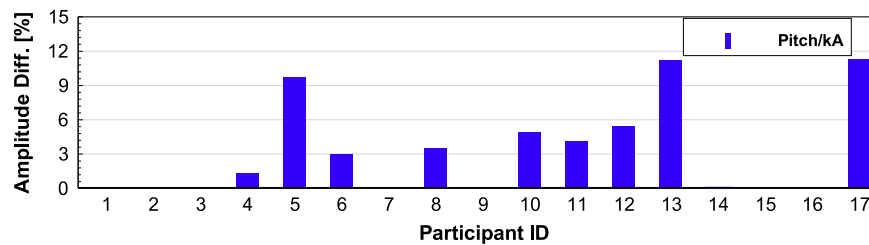**Fig. 19.** Amplitude differences of heave in NL2.

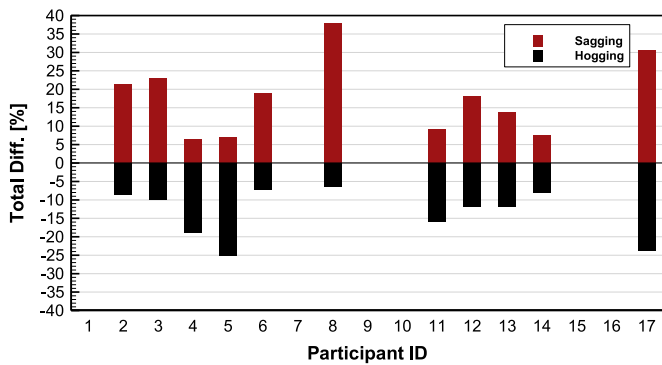**Fig. 20.** Amplitude differences of pitch in NL2.

Fig. 21. Total differences of hogging and sagging moments in NL2.

Participants 6, 11, 12, and 14 show smaller differences and Participants 4, 8, and 17 show larger differences in NL1.

3.3. Nonlinear response: NL2

The test case of NL2 is a highly nonlinear condition because nonlinear springing and slamming-whipping are expected owing to a large wave amplitude. The time series of heave and pitch are compared in Fig. 17. The time series are shifted to match the positive peaks of pitch motions at 0.0 s. A significant difference of heave is observed between the experimental and computational results. The heave of the experimental result is 30% larger than the average heave of the computational results. However, agreement between the experimental and computational results is quite good for pitch motion. In Fig. 18 (left), the time series of VBM at Section 4 are compared. A significant high frequency oscillation is observed, which can be corresponds to springing, whipping, or both. The high frequency oscillation increases the maximum sagging and hogging moments. The longitudinal distributions of sagging and hogging moments are compared in Fig. 18 (right). The statistical values are obtained from the maximum sagging and hogging moments of the numerical results. It should be noted that the sagging moments are highly increased by the high frequency oscillation. In addition, the standard deviation of the sagging moment is two times larger than that of hogging moment. The sagging moments of the experimental result are similar to those of the average of the computational results.

The amplitude differences of heave and pitch are compared in Figs. 19 and 20. The maximum differences of heave and pitch are about 27% and 11%, respectively. The maximum difference of heave is two times larger in NL2 compared to that in NL1. The total differences of sagging and hogging are compared in Fig. 21. The differences of sagging in NL2 are larger than those in NL1. Participants 4, 6, 11, 12, and 14 show smaller differences and Participants 5, 8, and 17 show larger differences in NL2.

3.4. Nonlinear response: NL3

The test condition of NL3 is selected to examine the effect of forward speed. The Froude number of NL3 is 0.12 whereas that of NL1 is 0.05. The time series of heave and pitch are compared in Fig. 22. The time series are shifted to match the positive peaks of pitch motions at 0.0 s. A significant difference of heave is observed between the experimental and computational results. The difference is about 30% between the experimental result and the average of the computational results. The time series of VBM at Section 4 are compared in Fig. 23 (left). High frequency oscillation is observed, but its magnitude is small. In Fig. 23 (right), the longitudinal distributions of sagging and hogging moments are compared. It should be noted that the maximum sagging moment is found at Section 5 ($x/L = 0.53$) in NL3, whereas it is found at Section 4 in NL1 and NL2. This is because of the increased forward speed. The experimental result shows good agreement with the average of the computational results.

The amplitude differences of heave and pitch are compared in Figs. 24 and 25. The maximum differences of heave and pitch are 23% and 10%, respectively. The total differences of sagging and hogging are compared in Fig. 26. Participants 4, 5, 8, and 17 show larger differences and the others show smaller differences in NL3.

3.5. Comparison of standard deviation

The standard deviations of the computational results are normalized by the average and compared with each other. Figs. 27 and 28 show the normalized standard deviations of heave and pitch. Both results show that the computational results are more scattered under a shorter wave period, larger wave amplitude, and faster forward speed. Fig. 29 shows a slightly different tendency in the result of VBM. The difference is that the standard deviation is also larger under longer wave periods. The standard deviations of nonlinear sagging and hogging moments are compared in Fig. 30. It is observed
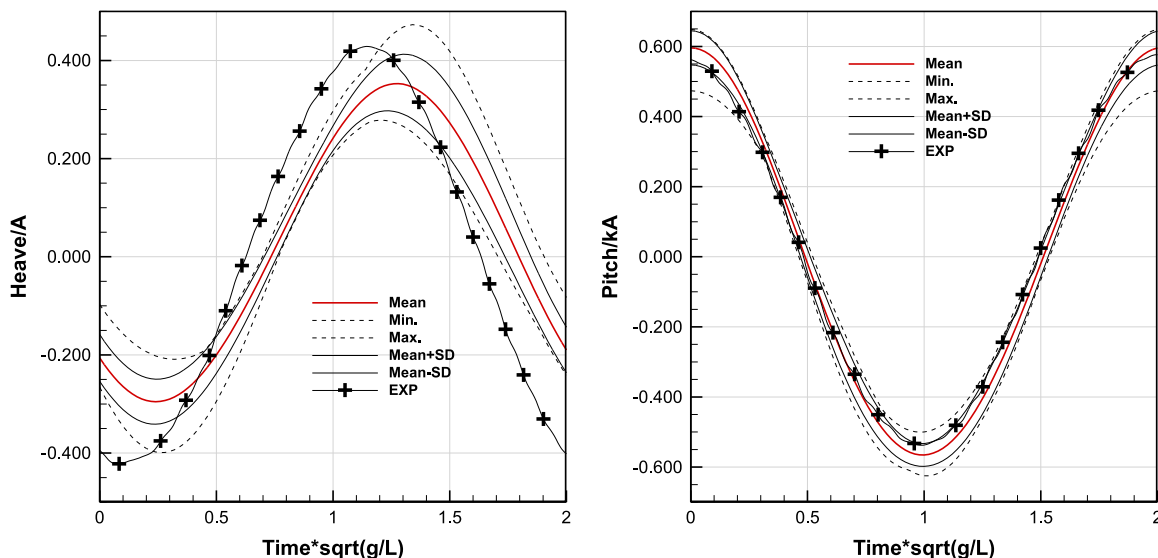

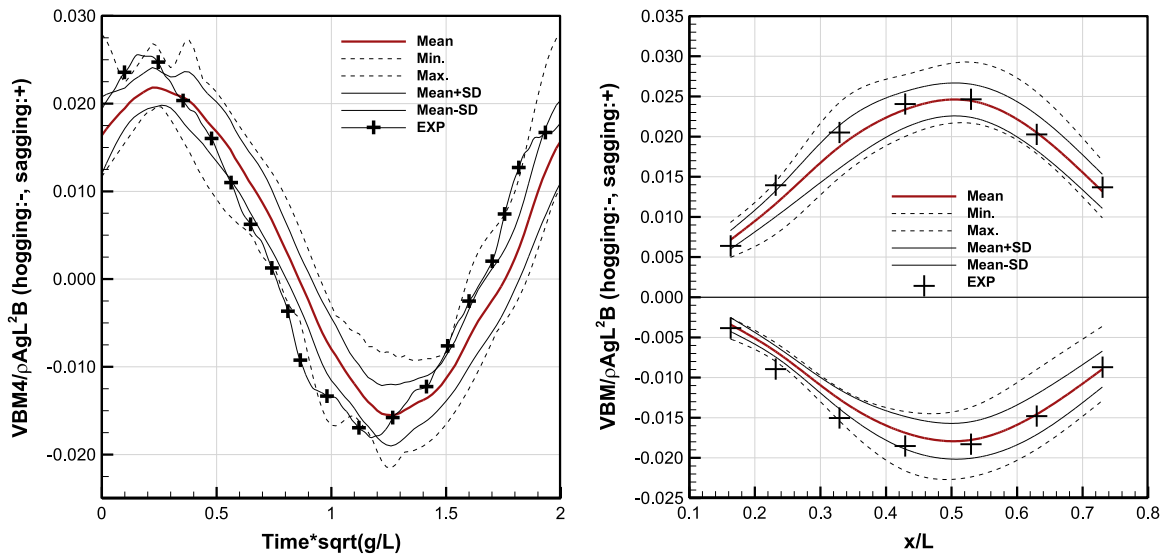**Fig. 22.** Comparison of heave and pitch in NL3.

Fig. 23. Comparison of VBM in NL3.
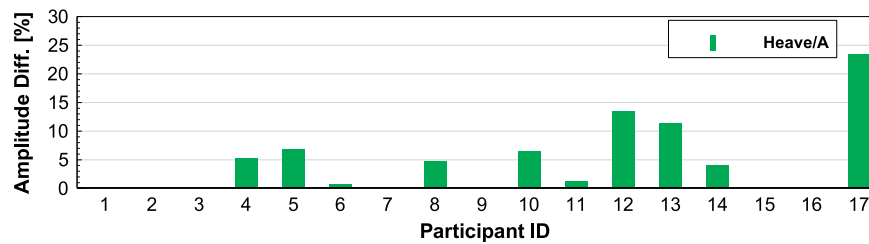

Fig. 24. Amplitude differences of heave in NL3.
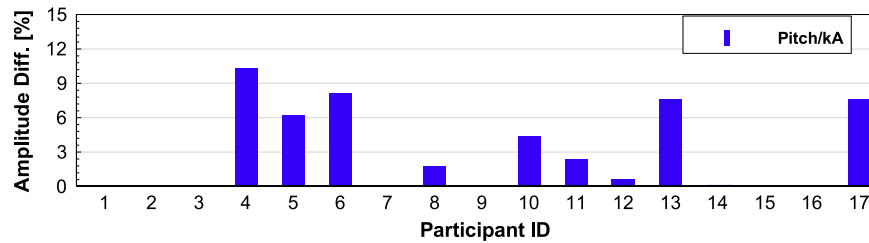

Fig. 25. Amplitude differences of pitch in NL3.

Fig. 26. Total differences of hogging and sagging moments in NL3.
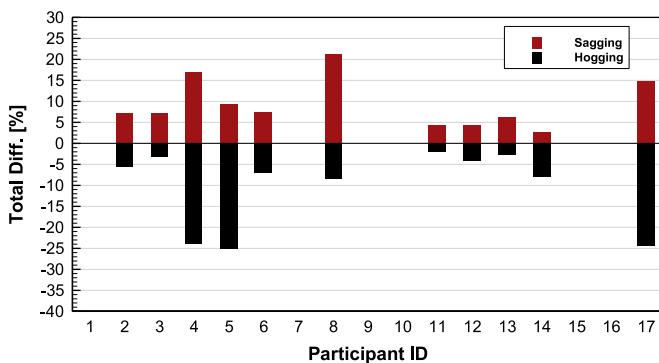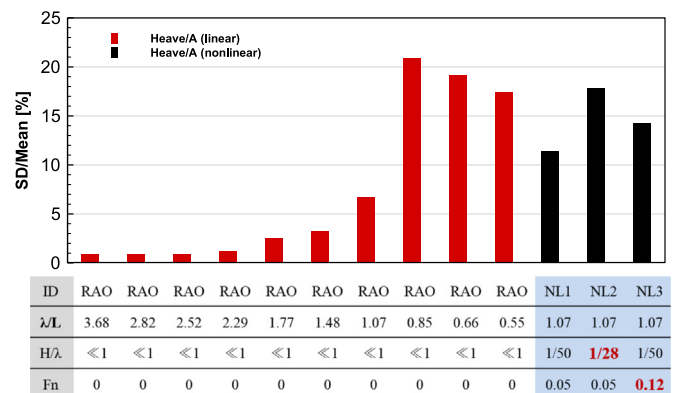

Fig. 27. Comparison of SD/Mean of heave.

that the computational results are more dispersed in NL2 compared to NL1 and NL3. The agreement between the computational results is the worst in hogging moments at $x/L=0.16$.

3.6. Comparison of difference by grouping

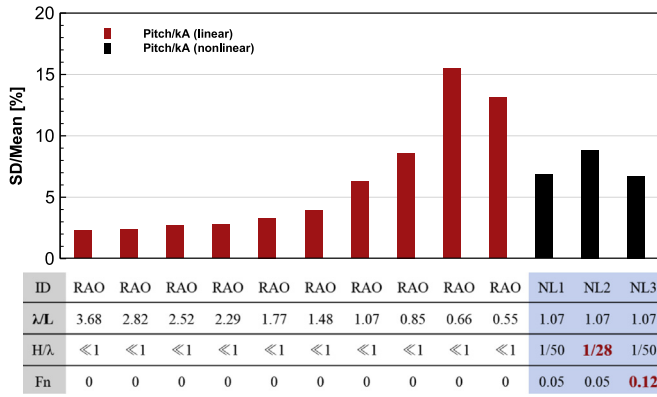The participants are categorized into three groups according to their base methods below.
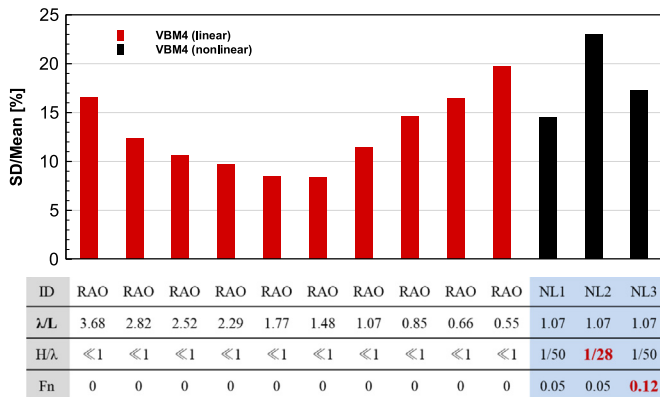
ID	RAO	RAO	RAO	RAO	RAO	RAO	RAO	RAO	RAO	RAO	NL1	NL2	NL3
λ/L	3.68	2.82	2.52	2.29	1.77	1.48	1.07	0.85	0.66	0.55	1.07	1.07	1.07
H/λ	≪1	≪1	≪1	≪1	≪1	≪1	≪1	≪1	≪1	≪1	1/50	**1/28**	1/50
Fn	0	0	0	0	0	0	0	0	0	0	0.05	0.05	**0.12**

Fig. 28. Comparison of SD/Mean of pitch.

ID	RAO	RAO	RAO	RAO	RAO	RAO	RAO	RAO	RAO	RAO	NL1	NL2	NL3
λ/L	3.68	2.82	2.52	2.29	1.77	1.48	1.07	0.85	0.66	0.55	1.07	1.07	1.07
H/λ	≪1	≪1	≪1	≪1	≪1	≪1	≪1	≪1	≪1	≪1	1/50	**1/28**	1/50
Fn	0	0	0	0	0	0	0	0	0	0	0.05	0.05	**0.12**

Fig. 29. Comparison of SD/Mean of VBM at Section 4.

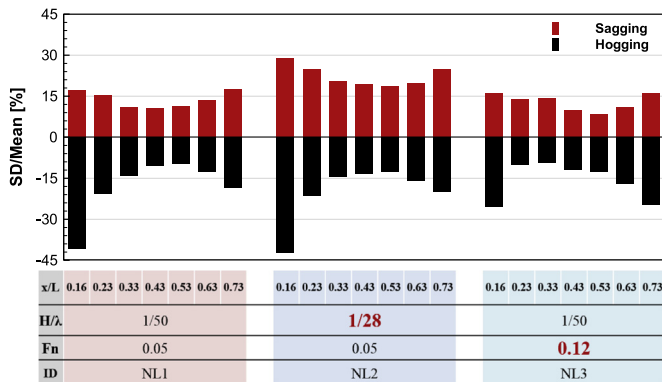| x/L	0.16	0.23	0.33	0.43	0.53	0.63	0.73		0.16	0.23	0.33	0.43	0.53	0.63	0.73		0.16	0.23	0.33	0.43	0.53	0.63	0.73
H/λ				1/50								**1/28**								1/50			
Fn				0.05								0.05								**0.12**			
ID				NL1								NL2								NL3			

Fig. 30. Comparison of SD/Mean of sagging and hogging moments.

- WGF: 3D BEM using wave Green's function, Participants 1, 3, 4, 6, 9, 16.
- RANKINE: 3D BEM using Rankine source, Participants 2, 11, 12, 13.
- STRIP: strip theory, Participants 5, 8, 15, 17.

The other participants are not grouped because the number of samples is too small to represent group characteristics. The RAO results are compared using a group difference calculation similar to that of the total difference. The group difference of the j-th component of the i-th group is calculated as

$$\text{Group Difference}_i^j \ [\%] = \frac{\sum_{k=1}^{N_i} \left| R_{i,k}^j - \text{Mean}^j \right|}{N_i * \text{Mean}^j} * 100$$

$(j = 1 \sim 10 : 0.54 \sim 3.68 \lambda/L)$ (5)

where $R_{i,k}^j$ is the computational result of the j-th component of the k-th member of the i-th group and N_i is the number of members of the i-th group. The group difference is not applied to the nonlinear responses because the grouping is not related to nonlinear extension.

Fig. 31 shows the comparison of heave in term of the group difference. The three groups show very small differences when $\lambda/L > 1.0$. It is observed that the group difference increases when $\lambda/L < 1.0$. Group STRIP shows a quite large difference in the region. A similar tendency is also observed in the comparisons of pitch and VBM, as shown in Figs. 32 and 33. The largest group difference is found in the result of Group STRIP and the smallest group difference is found in the result of Group RANKINE. Group RANKINE shows remarkably small group differences in the VBM results compared with the results of Groups WGF and STRIP.

4. Conclusions

Seventeen seakeeping analysis codes participated in the benchmark test for linear and nonlinear motion and load on the 6750-TEU containership. Statistical analysis is used for the comparison of the experimental and computational results. Findings and conclusions are as follows:

- The average of the computational results shows good agreement with the experimental result in terms of linear heave, pitch, and VBM.
- Compared to the experimental result, the numerical results tend to underestimate heave and VBM and overestimate pitch in nonlinear test conditions of NL1, NL2, and NL3.
- The maximum sagging moment is about 30% larger than the maximum hogging moment even in the mild sea condition of NL1.
- A significant high frequency oscillation is observed in NL2, which corresponds to springing, whipping, or both. Sagging moments are highly increased compared to hogging moments by the high frequency oscillation.
- The maximum sagging moment is found at Section 5 in NL3, whereas it is found at Section 4 in NL1 and NL2, which is from the increased forward speed.
- The computational results are more scattered for a shorter wave period, larger wave amplitude, and faster forward speed.
- The hogging moments of the computational results violently disperse near the stern ($x/L = 0.16$), whereas those do not near mid-ship and bow.
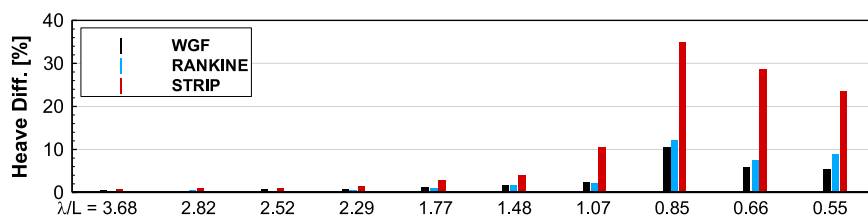

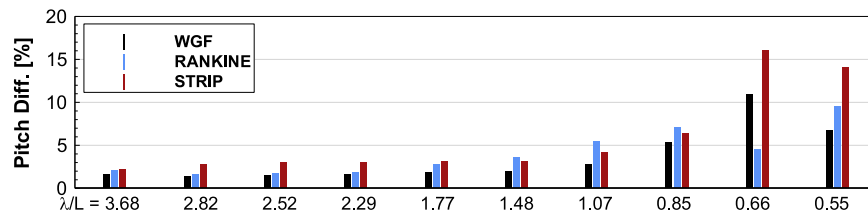**Fig. 31.** Comparison of heave difference by grouping.

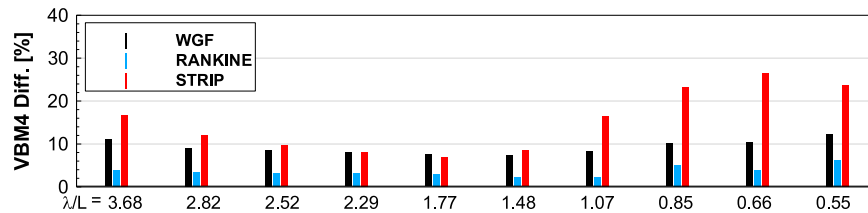**Fig. 32.** Comparison of pitch difference by grouping.

Fig. 33. Comparison of VBM difference by grouping.

- The largest group difference is found in the result of Group STRIP and the smallest group difference is found in the result of Group RANKINE.
- The scattered results might figure out what needs to be improved in the future. The scattered results of high frequency region or hogging moment near the stern might be related with numerical errors. On the other hand, the scattered responses in the larger wave or high forward speed might be related with theoretical limitations.

References

Belgova, M., 1962. Determination of overall bending moments caused by elastic vibrations of ships. Trans. of the Leningrad Institute of Water Transport.

Bishop, R.E.D., Price, W.G., 1979. Hydroelasticity of Ships. Cambridge University Press, London.

Bunnik, T., van Daalan, E., Kapsenberg, G., Shin, Y., Huijsmans, R., & Deng, G., 2010. A comparitive study on state-of-the-art prediction tools for seakeeping. In: Proceedings of the 28th Symposium on Naval Hydrodynamics, Pasadena, California.

Cummins, W.E., 1962. The impulse response function and ship motions. Schiffstechnik 9, 101–109.

Gentaz, L., Guillerm, P. E., Alessandrini, B., and Delhommeau, G., 1999. Three-dimensional free-surface viscous flow around a ship in forced motion. In: Proceedings of the 7th Int. Conf. Num. Ship Hydro., Paris, France, pp. 1–12.

Haskind, M.D., 1946. The hydrodynamic theory of ship oscillations in rolling and pitching. Prikl. Mat. Mekh 10, 33–66.

Havelock, T.H., 1942. The damping of the heaving and pitching motion of a ship. Philos. Mag. 33, 666–673, Ser. 7.

Hess, J.L., Smith, A.M., 1962. Calculation of Non-lifting Potential Flow About Arbitrary Three-Dimensional Bodies (No. ES-40622). Douglas Aircraft Company, Inc., Long Beach, CA.

Iijima, K., Yao, T., Moan, T., 2008. Structural response of a ship in severe seas considering global hydroelastic vibrations. Mar. Struct. 21, 420–445.

ITTC Seakeeping Committee, 1978. Report of the Seakeeping Committee. In: Proceedings of the 15th Int. Towing Tank Conference, The Hague, Netherlands, 1, pp. 55–114.

Jensen, J.J., Dogliani, M., 1996. Wave-induced ship hull vibrations in stochastic seaways. Mar. Struct. 9, 353–387.

Kashiwagi M., 1995. Prediction of Surge and its Effect on Added Resistance by Means of the Enhanced Unified Theory. Trans. West-Japan Society of Naval Architects, 89, pp. 77–89.

Kim, J.H., Kim, Y., Yuck, R.H., Lee, D.Y., 2015. Comparison of slamming and whipping loads by fully coupled hydroelastic analysis and experimental measurement. J. Fluids Struct. 52, 145–165.

Kim, Y., Kim, K.H., Kim, J.H., Kim, T., Seo, M.G., Kim, Y., 2011. Time-domain analysis of nonlinear motion responses and structural loads on ships and offshore structures-development of WISH programs. Int. J. Nav. Architect. Ocean Eng. 3 (1), 37–52.

Kim, Y., Kim, K.H., Kim, Y., 2009. Analysis of hydroelasticity of floating ship-like structures in time domain using a fully coupled hybrid BEM-FEM. J. Ship Res. 53 (1), 31–47.

Korsmeyer, F.T., Lee, C. H., Newman, J.N., & Sclavounos, P.D., 1988. The analysis of wave effects on tension-leg platforms. In: Proceedings of the 7th Conf. on Offshore Mech. and Arctic Eng., OMAE, Houston.

Korvin-Kroukovsky B.V., Jacobs W.R., 1957. Pitching and heaving motions of a ship in regular waves. Trans., SNAME, 65, pp. 590–632.

Kriloff A., 1896. new theory of the pitching motion of ships on waves, and of the stresses produced by this motion. Inst. Nav. Archit. Trans. 37, pp. 326–368.

Kring, D.C., 1994. Time Domain Ship Motions by a Three-dimensional Rankine Panel Method (Ph.D. dissertation). Mass Inst. of Technology, USA.

Lin, W.M., Yue, D.K.P., 1991. Numerical Solution for Large-amplitude Ship Motions in the Time Domain. National Academy Press, Washington D.C, pp. 41–66.

Malenica, S., and Tuitman, J.T., 2008. 3D FEM-3D BEM model for springing and whipping analysis of ships. In: Proceedings of the International Conference on Design and operation of Containerships, London.

Maruo, H., 1970. An Improvement of the Slender Body Theory for Oscillating Ships with Zero Forward Speed. 19. Bulletin of the Faculty of Engineering, Yokohama National University, pp. 45–56.

Nakos, D.E., Sclavounos, P.D., 1990. On steady and unsteady ship wave patterns. J. Fluid Mech. 215, 263–288.

Newman, J.N., 1964. A slender-body theory for ship oscillations in waves. J. Fluid Mech. 18 (4), 602–618.

Newman, J.N., and Sclavounos, P., 1980. The unified theory of ship motions. In: Proc. of the 28th Symposium on Naval Hydrodynamics, Tokyo.

Oberhagemann, J., Moctar, O., 2012. Numerical and experimental investigations of whipping and springing of ship structures. Int. J. Offshore Polar Eng. 22 (2), 108–114.

Ogilvie, T.F., Tuck, E.O., 1969. A Rational Strip Theory of Ship Motions: Part I. University of Michigan, Ann Arbor, Michigan.

Sadat-Hosseini, H., Wu, P.C., Carrica, P.M., Kim, H., Toda, Y., Stern, F., 2013. CFD verification and validation of added resistance and motions of KVLCC2 with fixed and free surge in short and long head waves. Ocean Eng. 59, 240–273.

Salvesen, N., Tuck, E.O., Faltinsen, O., 1970. Ship motions and sea loads. Transactions 78, 250–287.

Ursell, F., 1949. On the heaving motion of a circular cylinder on the surface of a fluid. Q. J. Mech. Appl. Math. 2 (2), 218–231.

Yang, K.K., Nam, B.W., Lee, J.H., Kim, Y., 2013. Numerical analysis of large-amplitude ship motions using FV-based Cartesian grid method. Int. J. Offshore Polar Eng. 23 (3), 168–196.